4th Imeko TC19 Symposium on Environmental Instrumentation and Measurements
Protecting Environment, Climate Changes and Pollution Control
June 3-4, 2013, Lecce, Italy

MICROSCALE DIELECTRIC BARRIER DISCHARGE PLASMA ACTUATORS: EXPERIMENTAL CHARACTERIZATION

Elisa Pescini [a,c], *Maria Grazia De Giorgi* [a], *Luca Francioso* [b], *and Antonio Ficarella* [a]

[a] Dep. of Engineering for Innovation, University of Salento, Via Monteroni, 73100 Lecce, Italy
[b] Istitute fot Microelettronics and Microsistems, IMM-CNR, Via Monteroni, 73100 Lecce, Italy
[c] elisa.pescini@unisalento.it

Abstract: Dielectric Barrier Discharge (DBD) plasma devices have been designed and manufactured with micro scale dimensions through photolithographic process on fiber glass substrate. AC operation under sinusoidal voltage up to 14 kV_{pp} and carrier frequency up to 2.5 kHz has been investigated experimentally by means of smoke flow visualizations and Particle Image Velocimetry. Velocity profiles, maximum induced velocity and induced body force have been calculated.
A comparison between the microactuator and a conventional macroactuator has been performed. It has been demonstrated that the microactuator produces velocities on the order of the macro scale actuator with a significant reduction in inception voltage, size and mass. This leads to a simpler and a less intrusive dispositive.

Keywords: Micro Plasma Actuator, Ionic wind, AC dielectric barrier discharge, Electrofluidodynamic (EFD)

1. INTRODUCTION

Dielectric barrier discharge plasma actuators (PA) modify a flow by providing an electronically controllable disturbance that brings to drag reduction, separation control, enhanced mixing, and noise suppression. They are easy to fabricate, have no moving parts and have low power requirements. Because of these features, they have received significant attention from the flow control community in recent years.
The configuration of the plasma actuator is simple, consisting of two electrodes separated by a dielectric layer: one electrode is supplied with high-voltage pulsed or AC excitation and exposed to the surrounding flow and one electrode is grounded and completely encapsulated by a dielectric material.
In presence of high- voltage pulsed or AC excitation, the gas located above the dielectric becomes weakly ionized creating a cold plasma discharge above the encapsulated electrode.
The plasma affects the flow by pumping momentum into the boundary layer region. Plasma imparts an electrodynamic (EHD) force on the surrounding fluid, inducing a 1–4 m/s wall jet occurring 0.5–1 [mm] above the dielectric surface.
The electrical and mechanical characteristics of a PA depend on various parameters such as electrode width, electrode thickness and dielectric layer thickness. Actuator performance is enhanced with decreasing the thicknesses of the exposed electrode and dielectric layer, going towards micrometric scale devices [1].
Computational codes demonstrated that, decreasing the electrode gap below 10 µm, there was a 10−100x increase in the induced force density [2, 3].
In this work, the performances of a micro plasma actuator in terms of induced thrust and velocity are evaluated.

2. EXPERIMENTAL ARRANGEMENT

A cross-sectional schematic of the DBD plasma actuator used in these experiments is shown in Fig. 1.
Both electrodes are realized with 35 µm thick electroplated copper, their streamwise width *w* is 1 mm and the electrode length *L* along the spanwise direction is 60 mm. The upper and lower electrodes are separated by a fiberglass dielectric layer (which thickness *t* is 0.8 mm) and they are shifted along the streamwise direction by a gap *g* equal to 250 µm.
The plasma actuator is located in the middle of a square flat plate, with a side length of 240 mm and a thickness of 5 mm. To reduce the effect of any external disturbance on the measurements, the tests are conducted in a closed box, made of Plexiglas (PMMA) to provide optical access. That is why measurements presuppose to start from the condition of quiescent air at atmospheric pressure. The box has the base coincident with the flat plate and his height is 240 mm. In all the work we will speak of zero position, upstream and downstream regions, with reference to Fig. 1.

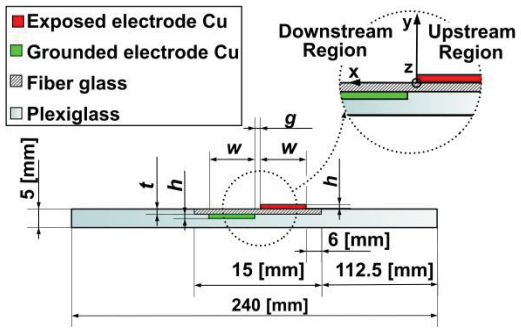

Fig. 1: Geometrical parameters of DBD plasma actuator

To power the plasma actuator, a high voltage amplifier (Trek 40-15) is used; a waveform generator card (NI-USB

6343) supplies various waveforms to the amplifier. In particular, the output of the amplifier is connected to the exposed electrode and the opposite electrode is grounded (see Fig. 2).
Throughout the experiments presented in this work, a sinusoidal waveform with voltage amplitude equal to 5 kV and a carrier frequency of 2.5 kHz is used.

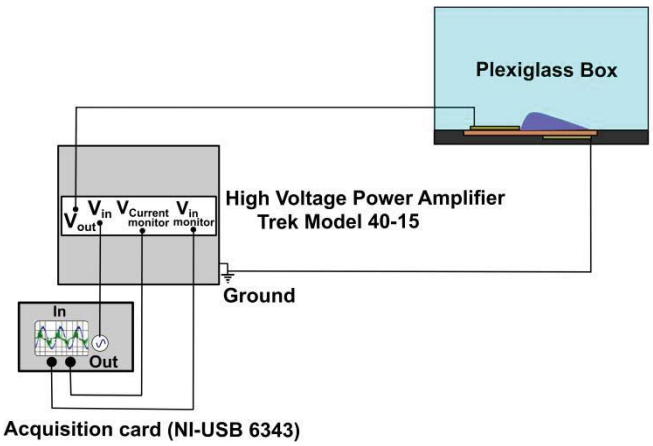

Fig. 2: Experimental setup

3. SMOKE VISUALIZATIONS

Flow images have been taken with the high-speed camera Memrecam GX-3 at a recording frequency of 250 KHz. Incense smoke has been used for filling the test chamber (Fig. 3).

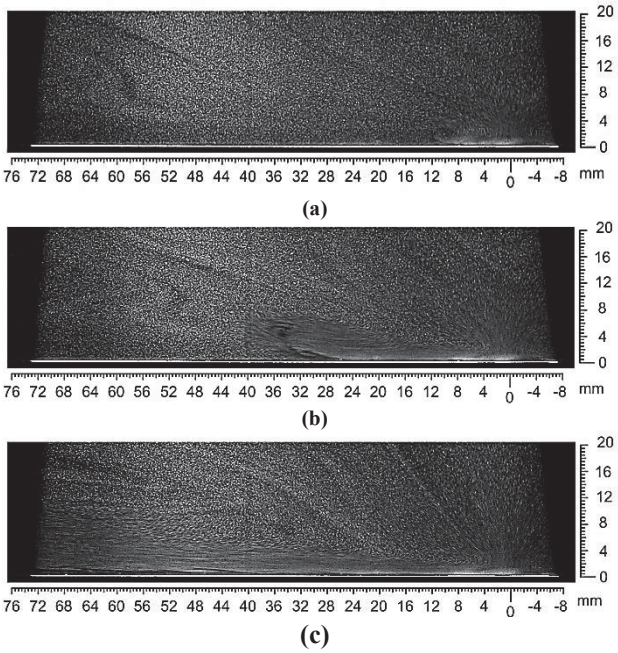

Fig. 3: Smoke Visualizations: (a) 2.6 s after actuation; (b) 3.5 seconds after actuation; (c) 4.8 seconds after actuation

Fig. 3 shows the region downstream the exposed electrode (see Fig. 1). It can be noticed that the flow is entrained by the plasma actuator and accelerated towards the grounded electrode.
In particular, it can be individuated a wall jet being formed on initiation of DBD plasma actuator, accompanied by a starting vortex (Fig. 3 (a)). The starting vortex rolls up, increases in size and travels along the wall [4]. The flow reaches a steady steady-state condition in approximately 5 seconds after the actuation (Fig. 3 (c)).

4. PARTICLE IMAGE VELOCIMETRY MEASUREMENTS

Particle Image Velocimetry (PIV) has been applied to characterize the flow field near the plasma actuator.
A two component PIV configuration has been chosen since the large span of the actuator ensures minimal 3D effects [5].
A Dantec 2D PIV system has been used to measure the flow field in the streamwise plane. The system consisted of a dedicated PC, a double pulse Nd: YAG laser (minimum power 200 mJ/pulse standard) and a FlowSense EO camera 4M with a 2048×2048 resolution. A Nikkor 60mm f/2.8 d A/F objective, set at an aperture of 4 has been used along with an extension ring Nikon PK13. PIV images processing has been performed using Dantec Dynamic Studio v3.0.
The camera captured a 20 mm x 20 mm zone, in particular 10 mm downstream the exposed electrode, 10 mm upstream and 20 mm along the y direction.
The Plexiglas box has been seeded with incense smoke (particle average diameter of 0.3 microns) reflecting the laser coherent light to the camera objective lens. The seeding has been adjusted in order to have at least 10 particles in each interrogation area. The duration between two successive frames has been set for each velocity to obtain a particle displacement equal to 25% of the interrogation area for all the measured velocities, which ensured that there was not signal dropout.
The recording frequency has been set to 6 Hz and 200 sets of dual pictures have been taken for each phased acquisition (synchronized with the Laser).
Various correlation methods, applied to the digital couples of images to compute the instantaneous vector fields, have been studied. The different methods have been compared in terms of number of vectors and in terms of percentage of bad vectors in respect to the total number of vectors given by the autocorrelation. It has been found that the Adaptive PIV using with an initial windows size equal to 128x128 and 2 refinement steps was the best method, thus this correlation algorithm has been applied to the couples of images to compute the instantaneous vector field.
Furthermore, other acquisitions have been performed in the same actuation conditions, analyzing them with the same correlation method (adaptive PIV using with an initial windows size equal to 128x128 and 2 refinement steps), but changing the acquisition parameters. In particular it has been noticed that increasing the number of the acquired images or starting the acquisition more than 10 second after actuation, leaded to the same velocity fields. Final results are shown for the PIV data given by the average the set of 200 images.

4.1 INDUCED FLOW FIELD

The vector map and the streamlines relative to the analyzed actuation case, sine wave with 5 kV amplitude and 2.5 kHz carrier frequency, are reported in Fig. 4.

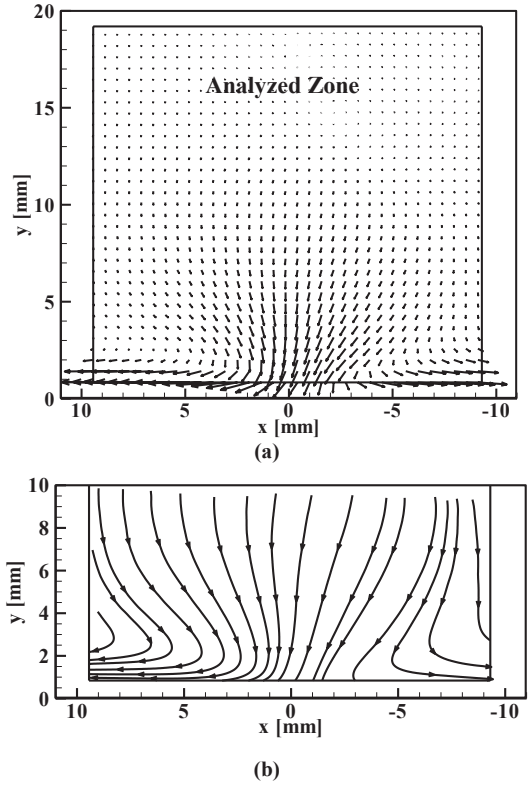

Fig. 4: Adaptive PIV 128x128 results in the analyzed zone: (a) Vector Map; (b) Streamlines close to the actuation zone

Due to the limtiations of the PIV technique in measuring close to the wall, further investigation will be made with Laser Doppler Velocimetry and hot wire measurements. Furthermore, very near to the wall (0.5-0.8 mm), there is almost the absence of particles because of the wall jet induced by the actuator (see Fig. 3 (c) and Fig. 5).

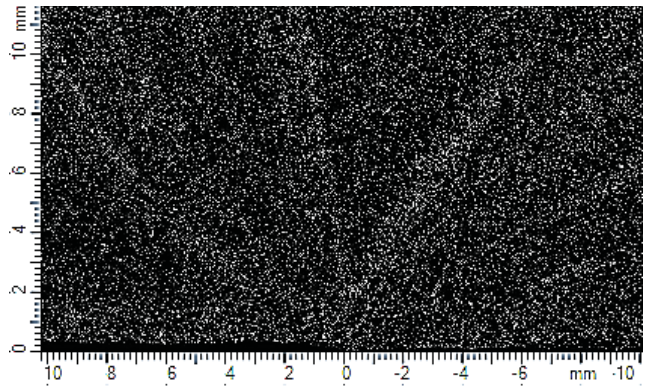

Fig. 5: Example of an acquired PIV image

The streamwise U and normal V velocity profiles, in sections at 0, 1, 3, 7 and 9 mm downstream the exposed electrode (the positions are referred to the zero position represented in Fig. 2), are reported in Fig. 6.

It can be noticed that the velocity increases moving downstream the exposed electrode. The maximum velocity is reached at x≈8 mm downstream the exposed electrode and at y≈0.85 mm from the wall. The maximum velocity magnitude is 1.36 m/s.

Downstream, at x=9 mm, the profile shows the transfer of momentum from the plasma to the air: the value of the maximum velocity decreases and the height of the profiles increases with increasing x values [6].

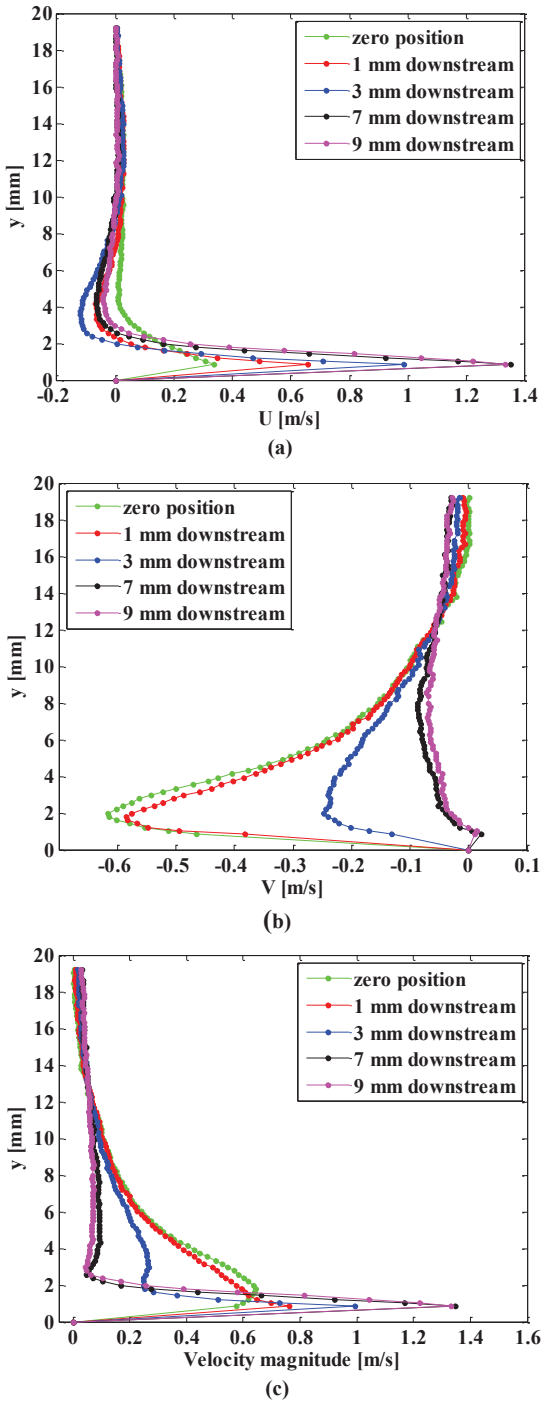

Fig. 6: Velocity profiles: (a) U velocity profiles; (b) V velocity profiles; (c) Velocity magnitude

4.2 ESTIMATION OF THE BODY FORCE

The data set from the high-speed PIV measurement is used for the thrust estimation, using the momentum balance equation in integral form, as proposed by different authors [5, 7, 8].
It involves the definition of a control volume. At the boundaries of the domain the momentum flux is calculated and equilibrium with the internal forces is assumed (see Fig. 7).

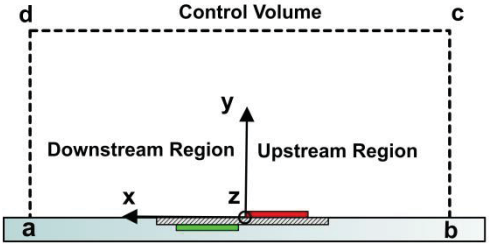

Fig. 7: The control volume for the momentum balance equations

In the flow visualizations it has been noticed that the steady state condition is reached in approximately 5 ms after actuation. As said in the previous section, increasing the number of the acquired images to more than 200 sets of dual pictures or starting the acquisition more than 10 second after actuation doesn't give difference in terms of velocity fields.
So, it is safe to use for the thrust estimation the PIV data given by the average the set of 200 images spanning from 10 s after the actuation to 43 s and to assume time independence.
A further assumption needs to be made, if the control volume boundaries are far enough from the bulk of the plasma body force (near the inner electrode edge) pressure can be considered uniform and equal [5, 7, 8].
Furthermore, since the large span of the actuator ensures minimal 3D effects [5], we can assume that there is not a big variation of velocity along the spanwise direction (z). With the assumptions of time independence, constant pressure and 2D flow, the application of the momentum balance equation on the control volume gives [9]:

$$\vec{F}=\oint_{abcd}\rho\vec{v}\,(\vec{v}\cdot\vec{n})dS \qquad (1)$$

where $\vec{F}$ is the sum of the forces applied to the control volume, $\vec{n}$ is the outward-facing normal vector at any point of its surface dS and $\vec{v}$ is the fluid velocity given by:

$$\vec{v}=\vec{U}+\vec{V} \qquad (2)$$

Equation (1) is developed for the boundaries of the control volume taking account of the no-slip condition at the wall. This implies that the momentum flux across the wall is zero.
Said L the electrode spanwise length, for an incompressible 2D flow, the two components of the total force per unit electrode length, are calculated as follows:

$$\frac{F_x}{L}=\rho\int_{da}|U|(\vec{v}\cdot\vec{n})dy+\rho\int_{cd}|U|(\vec{v}\cdot\vec{n})dx+\rho\int_{bc}|U|(\vec{v}\cdot\vec{n})dy \qquad (3)$$

$$\frac{F_y}{L}=\rho\int_{da}|V|(\vec{v}\cdot\vec{n})\,dy+\rho\int_{cd}|V|(\vec{v}\cdot\vec{n})\;dx+\rho\int_{bc}|V|(\vec{v}\cdot\vec{n})\,dy \qquad (4)$$

It should also be noted here that, for the x-direction, the calculated total force (F_x) contains the electrodynamic force due to the plasma $F_{x_{plasma}}$ and also the shear force between the flow and the surface $F_{x_{friction}}$, in particular:

$$F_x=F_{x_{plasma}}-F_{x_{friction}} \qquad (5)$$

A further simplification can be made, in particular, the flux over the c-d and b-c control volume boundaries is assumed to be negligible (quiescent air). In fact, in [5, 8] it was demonstrated that the major contribution to the induced force is generated by the wall jet, which leaves the CV across the left boundary d-a, as the maximum contribution to thrust comes from the velocity from section da.
This last simplification brings to:

$$\frac{F_x}{L}=\rho\int_{da}|U|(\vec{v}\cdot\vec{n})\,dy \qquad (6)$$

$$\frac{F_y}{L}=\rho\int_{da}|V|(\vec{v}\cdot\vec{n})\,dy \qquad (7)$$

In order to extract the reaction thrusts on the control volume, the integrals in the previous equations, have been numerically integrated in Matlab using the time-averaged PIV data. A trapezoidal rule has been used for the integration scheme. It has been chosen the surface c-b coinciding with the upstream section where the flow is not disturbed (quiescent air) and the surface a-d coinciding with the surface 9 mm downstream the exposed electrode. The height of the control volume has been chosen equal to 19.3 mm, which is the maximum height that we could resolve with the PIV acquisitions (Fig. 6). It can be observed that at y=19.3 mm the velocity is approximately zero (see Fig. 6), so the quiescent air hypothesis in the boundary c-d is valid.
Also, it is pertinent to note that a constant air density ρ has been assumed [7], equal to 1.2 kg/m^3.
Micro DBD performances have been calculated. The results from the micro scale actuators are compared with macro scale DBD actuator performances reported in literature [1, 10] and are summarized in Tab. 1.

Performance	Micro-DBD V=10 KV_{pp} f=2.5 KHz	Macro-DBD V=20 KV_{pp} f=1KHz [10]
Total force F_x per unit electrode length [$N\cdot m^{-1}$]	1.09E-03	3.9E-03
Maximum velocity magnitude v_{max} [$m\cdot s^{-1}$]	1.36	1.4
Total force F_x per unit actuator volume [$N\cdot m^{-3}$]	5.94E+02	6.84E+01
Total force F_x per unit actuator mass [$N\cdot g^{-1}$]	4.05E-01	4.10E-03
Velocity v_{max} per unit actuator volume [$m\cdot s^{-1}\cdot m^{-3}$]	1.24E+07	2.46E+04
Velocity v_{max} per unit actuator mass [$m\cdot s^{-1}\cdot g^{-1}$]	8.42E+00	1.44E-02

Tab. 1: Micro-DBD and macro-DBD actuator performances comparison

It can be concluded that employment of miniaturized electrodes allows the micro actuator to produce velocities on the order of macroscale actuators with a significant reduction in inception voltage, size, and mass. This leads to simpler and less intrusive integration of the dispositive in practical applications.

5. CONCLUSIONS

In this work AC operation under sinusoidal voltages with an amplitude equal to 5 kV and a carrier frequency of 2.5 kHz has been investigated experimentally by means of smoke flow visualizations and Particle Image Velocimetry. By means of the flow visualizations it has been found that the flow reaches a steady steady-state condition in approximately 5 seconds after actuation. PIV analysis has allowed determining the velocity profiles, maximum induced velocity and induced body force.

The developed microactuator has been compared with macroactuators and it has been found that employment of miniaturized electrodes allowed the microactuator to produce velocities on the order of macro scale actuators with a significant reduction in inception voltage, size, and mass. The comparison underlined that the micro scale actuators show an increase of both force and induced velocity per unit actuator mass and volume.

A dedicated activity will be devoted to MEMS technology adoption for electrodes fabrication on flexible Kapton foil and fiberglass FR4 substrates, and batch production of electrode array with photolithographic techniques. Micro fabrication technology will enable impressive cost reduction of actuators, easy integration of on-board electronics and future integration of high performance dielectric layers typically used in CMOS fabrication.

Through miniaturization of the DBD actuator geometries (both electrode size and electrode gap), we aim to demonstrate an increase in electric field and charge separation in an effort to improve the fluidic control authority and actuator effectiveness.

6. REFERENCES

[1] J. C. Zito, R. J. Durscher, J. Soni, S. Roy and D. P. Arnold, "Flow and force inducement using micron size dielectric barrier discharge actuators," *Applied Physics Letters,* vol. 100, 2012.

[2] S. Roy, D. Arnold, J. Lin, T. Schmitz, R. L. R. Durscher, J. Zito, D. Blood and C. Thompson, "Novel Plasma Actuators for Energy Efficiency," in *DARPA--Princeton Workshop, 22--24 August, 2011*.

[3] C.-C. Wang and S. Roy, "Microscale plasma actuators for improved thrust density," *Journal of Applied Physics,* vol. 106, 2009.

[4] R. Whalley and K.-S. Choi, "Starting, traveling, and colliding vortices: Dielectric-barrier-discharge plasma in quiescent air," *Physics of Fluids,* vol. 22, no. 091105, 2010.

[5] J. Kriegseis, C. Schwarz, C. Tropea and Grundmann, "Velocity-information-based force-term estimation of dielectric-barrier discharge plasma actuators," *Journal of Physics D: Applied Physics,* vol. 46, no. 055202 (13pp), 2013.

[6] M. Forte, J. Jolibois, J. Pons, E. Moreau, G. Touchard and M. Cazalens, "Optimization of a dielectric barrier discharge actuator by stationary and non-stationary measurements of the induced flow velocity: application to airflow control," *Experiments in Fluids,* vol. 43, no. 6, pp. 917-928, 2007.

[7] R. Durscher and S. Roy, "Evaluation of thrust measurement techniques for dielectric barrier discharge actuators," *Experiments in Fluids,* vol. 53, no. 4, p. 1165–1176, 2012.

[8] M. Kotsonis, S. Ghaemi, L. Veldhuis and F. Scarano, "Measurement of the body force field of plasma actuators," *J. Phys. D: Appl. Phys.,* vol. 44, no. 045204 (11pp), 2011.

[9] P. Hill and C. Peterson, Mechanics and Thermodynamics of Propulsion, Addison Wesley, Second Edition.

[10] T. Abe, Y. Takizawa and S. Sato, "Experimental Study for Momentum Transfer in a Dielectric Barrier Discharge Plasma Actuator," *AIAA Journal,* vol. 46, no. 9, pp. 2248-2256, September 2008.